NUMERICAL SIMULATION OF CO-COMBUSTION OF BIOMASS AND PULVERIZED COAL IN A PRECALCINER

by

Zhenliang WEI and Hongtao KAO*

College of Materials Science and Engineering, Nanjing Tech University, Nanjing, China

Original scientific paper
https://doi.org/10.2298/TSCI240722263W

As high energy consumption and pollution increase in the cement industry, utilizing biomass as a substitute fuel has been deemed a promising energy-saving and emission reduction measure. Currently, research on the mixed burning of coal and biomass has mostly been done at the experimental level, providing limited guidance for actual production. Therefore, this paper investigates the mixed burning of coal fines and corn straw in a TTF-type precalciner by combining real production data and CFD numerical simulation methods. The influences of different corn straw blending ratios on the performance of precalciner are explored. The results show that, compared with non-corn straw, as the blending ratio of corn straw increases, the high temperature zone inside the precalciner significantly shrinks. The maximum temperature of the furnace decreases to 1370 K, the export raw material's decomposition rate decreases to 83.92%, and the concentration of NO drops to 464 ppm when 40% corn straw is blended. After comprehensive consideration, it is found more suitable to mix 30% corn straw. Compared to experimental studies, this study has more practical guidance significance for cement enterprises seeking to utilize biomass alternative fuels.

Key words*: biomass, alternative fuel, mixed combustion, precalciner, numerical simulation*

Introduction

Cement production, a high energy consumption and pollution process, consumes approximately 12%-15% of overall industrial energy consumption and constitutes around 7% of total global carbon emissions [1, 2]. Furthermore, cement production generates significant amounts of NO_x, SO_2, and PM, which worsen air quality and the ecological environment [3, 4]. Reducing energy consumption and pollution emissions while maintaining production capacity is vital in the cement industry. Among various strategies, utilizing alternative fuels is often regarded as one of the most promising techniques for saving energy and reducing emissions. This approach can significantly reduce dependence on fossil fuels and decrease greenhouse gas and pollutant emissions [5, 6].

Among numerous alternative fuels, biomass has received much attention due to its renewability [7] and low carbon characteristics [8]. As one of the countries with the richest biomass resources in the world, China produces about 1.04 billionns of various agricultural waste annually [9]. These considerable biomass resources have enormous development potential. The application of biomass as a substitute fuel in the cement industry has various advantages. First, biomass features low carbon, low nitrogen, and low pollution [10]. Second, biomass has a

* Corresponding author, e-mail: kaoht@163.com

higher volatile content and a faster combustion rate. Its high volatility allows it to release large amounts of volatile gases during heating. When co-combusted with coal, it can improve fuel ignition performance and effectively enhance combustion efficiency. Additionally, it can enhance the combustion characteristics of pulverized coal, thereby reducing instability during the combustion process [11, 12].

Currently, there have been many studies on biomass combustion and its co-combustion with coal. Yi *et al.* [12] utilized thermogravimetric analysis to investigate coal and biomass co-combustion in an O_2/CO_2 atmosphere. The study found that blending biomass improves coal combustion efficiency. Co-combustion of various biomass and coal had a considerable boosting effect, but the influence between different biomass was limited. Sun *et al.* [13] simulated the mixed combustion of coal and biomass in a 300 MW coal fines boiler. They discovered that that the co-combustion process reduced the peak temperature within the furnace and significantly decreased NO_x emissions. Jeong *et al.* [14] studied the kinetic characteristics of pyrolysis after blending coking coal and biomass. They found that as the ratio of biomass mixing increased, the reactivity of the coal-biomass mixture increased, and the reaction activation energy decreased. Li *et al.* [15] investigated the effect of co-pyrolysis of coal and biomass in an inert atmosphere on nitrogen and sulfur release. They observed that the release of volatiles exhibited significant synergistic effects within the temperature range of 600-800 °C. Yuan *et al.* [16] used a thermal analyzer to examine the mixed combustion properties of clean coal and biomass particles. They discovered that mixed combustion improves combustion performance, with a significant synergistic effect between the two. Mikulčić *et al.* [17] simulated three co-combustion scenarios of coal fines and waste wood in a precalciner. They observed that mixed combustion decreases pollutant emissions. Ghenai *et al.* [18] conducted a numerical simulation study on the co-combustion of coal and biomass, and found that co-combustion can reduce NO_x and CO_2 emissions. Wang *et al.* [19] conducted a numerical simulation study on biomass co-combustion under the oxy-MILD mode. The study found that the oxy-MILD combustion mode is more effective in reducing NO_x emissions. Jia *et al.* [20] investigated the co-combustion of biomass and coal gangue and found that this process can reduce NO and SO_2 emissions. Black *et al.* [21] simulated the combustion of coal and biomass in a 500 MWe coal-fired boiler and explored the potential impact of fuel type and combustion atmosphere on boiler heat transfer characteristics. Kim *et al.* [22] research found that the mixture of coal and ash-free biomass exhibited the best combustion performance. Oladejo *et al.* [23] and Chansa *et al.* [24] studies found that coal and biomass co-combustion exhibited a synergistic effect.

The aforementioned review demonstrates that the majority of research on the co-burning of coal and biomass are conducted at the experimental level. However, the cement precalciner is a large reactor accompanied by numerous complex reactions, such as fuel combustion and coupled raw material decomposition [25]. This complexity making it challenging to investigate under laboratory conditions. Furthermore, experimental studies alone are insufficient to effectively guide actual cement production. Currently, there is limited research on the co-burning of coal powder and biomass in precalciner, which hinders the application of biomass in the cement industry. Based on the aforementioned research's insufficiency, this study combines actual production data. It employs CFD numerical simulation methods to investigate the simultaneous burning of coal powder and corn straw in a *TTF*-type precalciner. The effects of different corn straw blending ratios on the temperature field, composition field, raw material decomposition, and NO_x compounds in the decomposition furnace are examined and analyzed in detail. The aim is to determine the optimal corn straw blending ratio under permissible production conditions, providing technical guidance for practical production.

Simulation methods and mathematical models

Fundamental conservation equation

The combustion of coal fines is highly complex [26], and any flow problem must adhere to the laws of mass and momentum conservation [27]. Furthermore, in systems involving heat exchange, the law of energy conservation must also be followed. The corresponding equations are:

– Mass conservation equation

$$\frac{\partial(\rho)}{\partial t}+\frac{\partial(\rho u)}{\partial x}+\frac{\partial(\rho v)}{\partial y}+\frac{\partial(\rho w)}{\partial z}=0 \tag{1}$$

where u, v, and w [ms^{-1}] are the velocity components in the x-, y-, and z- directions, respectively, t [s] – the time, and ρ [kg/m^3] – the density.

– Momentum conservation equation

$$\begin{aligned}
&\frac{\partial(\rho u)}{\partial t}+\mathrm{div}(\rho u\vec{\mathrm{v}})=div(\mu\mathrm{grad}u)-\frac{\partial p}{\partial x}+S_u\\
&\frac{\partial(\rho v)}{\partial t}+\mathrm{div}(\rho v\vec{\mathrm{v}})=div(\mu\mathrm{grad}v)-\frac{\partial p}{\partial y}+S_v\\
&\frac{\partial(\rho w)}{\partial t}+\mathrm{div}(\rho w\vec{\mathrm{v}})=div(\mu\mathrm{grad}w)-\frac{\partial p}{\partial z}+S_w
\end{aligned} \tag{2}$$

where μ is the dynamic viscosity, p – the pressure on the fluid element, and S_u, S_v, and S_w are the source terms in the x-, y-, and z-directions, respectively. These source terms include body force sources, fluid dynamic sources, and user-defined sources.

– Energy-conservation equation

$$\rho c_p\left(\frac{\partial T}{\partial t}+\vec{\mathrm{u}}\nabla T\right)=\nabla(k\nabla T)+\Phi+q_{\mathrm{rad}}+q_{\mathrm{gen}} \tag{3}$$

where c_p [Jkg^{-1}K^{-1}] is the specific heat capacity at constant pressure, T [K] – the temperature, $\vec{\mathrm{u}}$ – the fluid velocity vector, k [Wm^{-1}K^{-1}] – the thermal conductivity, Φ – the viscous dissipation term, q_{rad} [Wm^{-3}] – the radiation term, and q_{gen} [Wm^{-3}] – the internal heat source term.

Gas-phase turbulence model and particle motion model

Considering the possibility of complex flows such as secondary flow and swirl within the precalciner. This study employs the realizable k-ε model with swirl correction [28], which effectively simulates complex flows such as secondary flow and swirl. The k represents turbulent kinetic energy, while ε represents its dissipation rate. The standard equation for the k-ε model is:

$$\frac{\partial(\rho k)}{\partial t}+\frac{\partial(\rho k\mu_i)}{\partial x_i}=\frac{\partial}{\partial x_j}\left[\left(\mu+\frac{\mu_t}{\sigma_k}\right)\frac{\partial k}{\partial x_j}\right]+G_k+G_b-\rho\varepsilon-Y_M+S_k \tag{4}$$

$$\frac{\partial(\rho\varepsilon)}{\partial t}+\frac{\partial(\rho\varepsilon\mu_i)}{\partial xi}=\frac{\partial}{\partial x_j}\left[\left(\mu+\frac{\mu_t}{\sigma_\varepsilon}\right)\frac{\partial\varepsilon}{\partial x_j}\right]-C_{2\varepsilon}\rho\frac{\varepsilon^2}{k}+C_{1\varepsilon}\frac{\varepsilon}{k}(G_k+C_{3\varepsilon}G_b)+S_\varepsilon \tag{5}$$

where G_b is the buoyancy-induced turbulent kinetic energy and G_k – the average velocity gradient-driven turbulent kinetic energy. The impact of pulsation expansion in compressible turbulent flow is represented by Y_M. The Planck constants for dissipation rate and turbulent kinetic

energy, respectively, are σ_k and σ_ε, S_k and S_ε are specified source terms, and $C_{1\varepsilon}$, $C_{2\varepsilon}$, and $C_{3\varepsilon}$ are the empirical constants.

In this work, the motion of the particles inside the furnace is simulated employing the discrete phase model (DPM). The DPM is based on a stochastic trajectory model from the Lagrangian perspective and simulates the motion process of particles [29]. The motion equation for particles under the random orbit model is:

$$\frac{\mathrm{d}u_p}{\mathrm{d}t} = F_D\left(u - u_p\right) + \frac{\mathrm{g}_x\left(\rho_p - \rho\right)}{\rho_p} + F_x \tag{6}$$

where $F_D(u - u_p)$ [Nkg^{-1}] is the gravitational force exerted on particles per unit mass, u [ms^{-1}] – the gas phase velocity, ρ_p [kgm^{-3}] – the density of particles, g_x [ms^{-2}] – the acceleration due to gravity, and F_x [N] – the sum of all forces acting on a particle, except for gravity and gravitational force.

Particle combustion model

Upon entering the furnace, coal fines and biomass undergo thermal decomposition, releasing volatile substances and producing coke. This work simulates the precipitation of volatile components in coal fines and biomass using a two-step competition rates model. The model adopts a segmented solution method to obtain the precipitation rate of volatile matter in different temperature ranges, and its expression is [30]:

$$R_1 = A_1 \mathrm{e}^{-\left(E_1/\mathrm{R}T_p\right)} \tag{7}$$

$$R_2 = A_2 \mathrm{e}^{-\left(E_2/\mathrm{R}T_p\right)} \tag{8}$$

where R_1 and R_2 are the competitive reaction rate coefficients obtained by controlling volatilization analysis under different temperature ranges. The combustion of leftover coke after volatilization analysis is simulated employing the kinetics/diffusion-limited reaction rate model. The pace at which oxygen molecules arrive at the coke surface, D_0, and the rate at which coke and O_2 molecules react, K, once they do so both affect the coke's combustion rate [31]. The expression for this model is given:

$$\frac{\mathrm{d}m_p}{\mathrm{d}t} = -A_p P_{\mathrm{OX}} \frac{D_0 K}{D_0 + K} \tag{9}$$

$$D_0 = C_1 \frac{\left(\dfrac{T_P + T_\infty}{2}\right)^{0.75}}{d_p} \tag{10}$$

$$K = C_2 \mathrm{e}^{-\left(E_2/\mathrm{R}T_p\right)} \tag{11}$$

where A_p is the particle's surface area, P_{OX} – the gas surrounding the particle's partial pressure, d_p – the particle's size and the temperatures of the surrounding gas, and the starting particle are denoted by T_∞ and T_P, respectively.

Raw material decomposition

For raw material decomposition, the decomposition of $CaCO_3$ is simulated utilizing the species transport model and the Finite rate/eddy dissipation model. The conservation equation for component transport:

$$\frac{\partial}{\partial_t}\left(\rho Y_i\right)+\nabla\left(\rho\vec{v}Y_i\right)=-\nabla J_i+R_i+S_i \tag{12}$$

where Y_i is the mass fraction of substance i, R_i – the net rate of chemical reactions is represented, S_i – the rate of additional generation from discrete phase and user-defined source terms is represented, and J_i – the diffusion flux of substance i.

The decomposition reaction equation of $CaCO_3$ is expressed:

$$CaCO_3(s)\rightarrow CaO(s)+CO_2(g),\ \Delta H=+178\ \text{KJ/mol} \tag{13}$$

This equation is used to determine the rate of raw material decomposition:

$$\omega=\frac{\dot{m}_1-\dot{m}_2}{\dot{m}_1}\times 100\% \tag{14}$$

where the raw material inlet's total mass-flow rate of $CaCO_3$ is represented by $\dot{m}_1$, the mass-flow rate of exit $CaCO_3$ is indicated by $\dot{m}^2$.

The NO_x generation model

Regarding combustion, the generation of NO_x is mainly classified into three types: prompt NO_x, thermal NO_x, and fuel NO_x. The FLUENT provides models for these three types of NO_x generation. Considering that the amounts of prompt NO_x and thermal NO_x generated in the precalciner are minimal. This study mainly focuses on fuel NO_x to simulate the formation of NO_x in the precalciner. Figure 1 shows the pathways for the generation of fuel NO_x. It is primarily assumed that the nitrogen in the fuel comes from volatiles and char. The nitrogen in the char can be directly converted to NO, while the nitrogen in the volatiles needs to be converted to NO via the intermediate HCN.

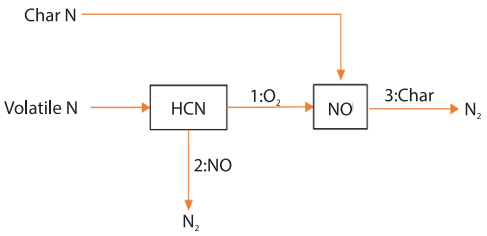

Figure 1. Fuel NO_x generation pathway

Solution methods

This study uses ANSYS FLUENT software for numerical simulations, employing the finite volume method to solve the governing equations. The CFD code was used to solve the mathematical model. The SIMPLE algorithm is used for pressure-velocity coupling, and all discretization schemes are second-order upwind.

Basic information

Geometrical model and grid

This study focuses on the TTF-type precalciner of a 5000 tonne per day cement clinker production-line in actual operation. The geometric model of the furnace is illustrated in fig. 2, which consists of a bottom cone, two necked portions, and three cylinders. The total height of the furnace is 45.88 m, with a maximum diameter of 7.1 m. The lower cone has a height of 5.6 meters, while the lower, middle, and upper columns have heights of 9.1 m, 12.9 m,

and 8.22 m, respectively. Four raw material pipes are symmetrically distributed on the middle and lower columns, with two pipes on each column. Two tertiary air ducts are symmetrically positioned above the interface between the lower cone and lower column. Additionally, four coal (biomass) injection ducts are symmetrically placed above the tertiary air ducts.

A hexahedral grid structure was adopted for the precalciner simulation. Compared to tetrahedral meshes, hexahedral meshes offer better computational accuracy, mesh quality, computational efficiency, and stability. A non-uniform meshing strategy was employed in the model, with mesh refinement applied to specific regions (inlet and outlet) to ensure computational accuracy. Through multiple trials, the optimal number of mesh elements was selected to both maintain accuracy and reduce computational cost. To ensure grid-independent results, a grid independence study was conducted using five grid numbers: 818800, 913200, 1032000, 1104840, and 1216580. The predicted average outlet temperatures were compared with the actual outlet temperature, as presented in tab.1. The results demonstrated that a grid number of 1032000 provided the closest agreement with the actual outlet temperature. Further increases in grid number yielded negligible changes in the predicted temperature. Consequently, the 1032000-grid configuration, depicted in fig. 3, was selected for subsequent simulations. All mesh qualities have a determinant $2 \times 2 \times 2 > 0$, with the minimum being 0.45 and the smallest angle being 32°. This fully meets the computational accuracy requirements.

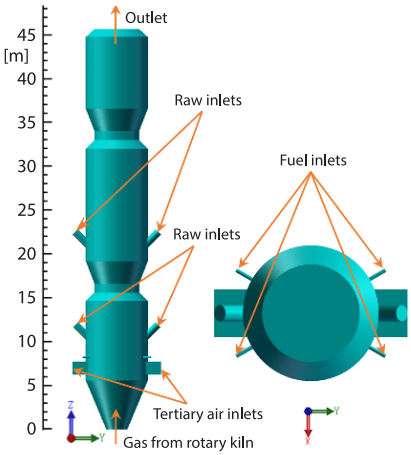

Figure 2. Schematic diagram of the geometric model of the precalciner

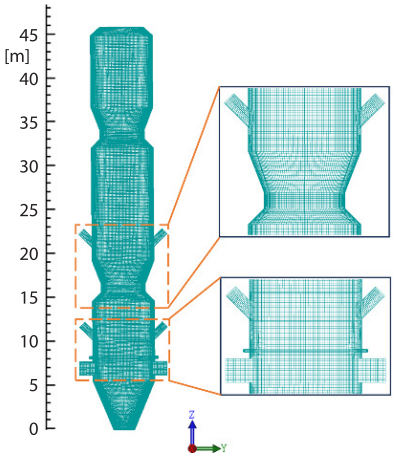

Figure 3. Schematic diagram of the precalciner grid

Table 1. Average and actual temperatures at the outlet of precalciner with varying grid numbers

Number of grids	818800	913200	1032000	1104840	1216580
Simulated temperature [K]	1120	1134	1154	1152	1150
Actual temperature [K]	1181	1181	1181	1181	1181

Material characteristics and boundary factors

The results of these analyses for coal and corn straw are presented in tab. 2, while the chemical compositions of the raw materials are listed in tab. 3. Powdered coal has particle sizes ranging from 5 μm at the least to 90 μm at the maximum and 65 μm at the average. The pulverized coal particles are spherical, with a density of 1400 kg/m^3, a specific heat capacity of

1100 J/kgK, a volatile release temperature of 400 °C, a particle expansion coefficient of 1.1, and an initial temperature of 337 K. The raw material's smallest, maximum, and average particle sizes are 20 μm, 60 μm, and 45 μm, respectively. The density of $CaCO_3$ particles is 2800 kg/m^3, the specific heat capacity is 856 J/kgK, the thermal conductivity is 2.25 W/mK, and the initial temperature is 1040 K. A fixed particle size of 200 μm was assumed for the corn straw.

Table 2. Coal and corn straw industrial and elemental analyses

Sample	Industry analysis [%]				Elemental analysis [%]					$Q_{net,ar}$ [MJkg^{-1}]
	M_{ad}	A_{ad}	V_{ad}	FC_{ad}	C_{ad}	H_{ad}	O_{ad}	N_{ad}	S_{ad}	
Coal	2.92	20.33	29.00	47.75	64.23	3.77	29.92	0.93	1.15	24.09
Corn straw	10.26	3.97	70.51	15.26	49.21	6.37	43.63	0.58	0.21	15.48

where M is the moisture, A – the ash, V – the volatile, FC – the fixed carbon, an subscript ad – the air-dry basis.

Table 3. Chemical composition of the raw materials

Sample	SiO_2	Al_2O_3	Fe_2O_3	CaO	MgO	Loss
Raw material [%]	11.76	3.69	2.76	42.83	1.30	35.28

Five sets of operating conditions were established based on varying proportions of coal powder mixed with corn straw. The initial mass-flow rate of pulverized coal was 4.8 kg/s, with corn straw replacing some of it in equal mass ratios (0%,10%, 20%, 30%, and 40%). Only the mass-flow rates of coal powder and corn straw being altered while all other operating parameters remained constant. The raw material inlet was specified as a mass-flow inlet with a flow rate of 16.8 kg/s. The initial pressure is –2565 Pa, the turbulence intensity is 10%, and the hydraulic diameter is 0.85 m.The tertiary air velocity and temperature were set to 28 m/s and 1300 K, respectively. The excess air coefficient is 1.189. The initial pressure is –348 Pa, the turbulence intensity is 10%, and the hydraulic diameter is 1.875 m. The kiln tail gas velocity and temperature were specified as 30 m/s and 1370 K, respectively. The initial pressure is –587 Pa, the turbulence intensity is 10%, and the hydraulic diameter is 2.4 m. A pressure outlet boundary condition was employed, with the exit pressure set at –1000 Pa. The backflow temperature is set to 1100 K, the backflow turbulence intensity is set to 10%, and the backflow hydraulic diameter is 5.1 m. The precalciner wall was assumed to be insulated. The main components of the rotary kiln exhaust gas were 11.3% CO_2, 1.0% O_2, 0.5% CO, and 87.2% N_2. Under these conditions, no biomass was used in the rotary kiln.

Model verification

To assess the reliability of the simulation results, a comparison was performed between the predicted outlet values and the measured values obtained from the thermal calibration of the precalciner, as presented in tab. 4. The error between the simulated and measured values was found to be less than 5%, which falls within the acceptable range for engineering applications. This agreement confirms the reliability of the simulation results. Figure 4 shows the residual curves from the model calculations. As can be seen from the figure, after 2000 steps, the low-

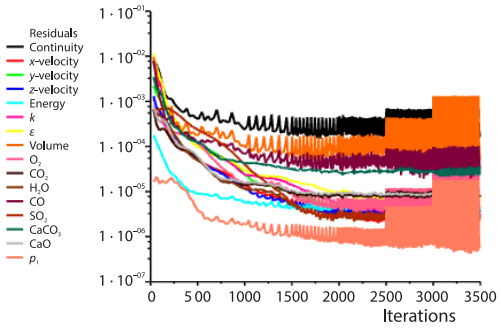

Figure 4. Residual curve of the calculation

est points of each curve are nearly aligned. The residuals are all less than 10^{-3}, indicating that the computation has converged. This further confirms the reliability of the simulation results.

Table 4. Comparing the measured and simulated values at the precalciner 's outlet

Parameter	Biomass [%]	Simulation value	Measured value	Error [%)]
Temperature [K]	0	1154	1181	2.29
CO_2 content [%]	0	25.44	26.3	3.27
O_2 content [%]	0	2.39	2.44	2.05

Simulation results and discussion

Combustion simulation under different corn straw blending ratios

Influence on the temperature field

Figure 5 illustrates the temperature contour map of the $x = 0$ section in the precalciner with varying proportions of corn straw. The figure demonstrates that the high temperature zone within the furnace is concentrated between the upper and lower raw material pipes and the lower cone section, exhibiting a symmetrical temperature distribution. The elevated temperatures between the upper and lower raw material pipes can be attributed to this region being the primary combustion area for the fuel, with ample oxygen supply. Upon entering the furnace, the coal powder and corn straw rapidly release volatile substances, and the volatile matter and fixed carbon undergo intense combustion, resulting in higher temperatures. The high temperature flue gas coming from the kiln tail is what causes the high temperature in the lower cone section. The temperature distribution between the upper and lower raw material pipes exhibits higher temperatures on both sides and relatively lower temperatures in the central region. This is because the majority of the raw material from the lower raw material pipe decomposes in this middle area. The decomposition process of the raw material necessitates the absorption of a substantial amount of heat, leading to comparatively lower temperatures in the central section. Furthermore, as the proportion of corn straw replacing coal powder increases, the high temperature zone between the upper and lower raw material pipes progressively narrows. Without biomass, the highest temperature in the precalciner is 1600 K. When 40% corn straw is added, the maximum temperature gradually decreases to 1370 K. Similarly, Sun *et al.* [13] in their study on the co-combustion of biomass and coal in a pulverized coal boiler also found that co-combustion reduced the peak temperature inside the furnace. The temperatures in the middle and upper columns also exhibit a slight decrease with the increasing proportion of corn straw replacing coal powder. The temperature at the precalciner outlet decreases from 1148 K without biomass to 1141 K when 40% corn straw is blended.

Figure 6 shows the average gas temperature at different heights in the precalciner when blending different proportions of corn straw. The figure reveals that, irrespective of the corn straw blending ratio, the furnace exhibits a consistent temperature change trend, characterized by an initial decrease, followed by an increase, and subsequently a decrease. This occurs because, after the flue gas from the kiln tail enters the furnace, the space rapidly expands, causing the average temperature to drop. Then, as the coal and corn stalks combust, the temperature quickly rises. Finally, the raw material entering the furnace from the upper feed pipe absorbs a large portion of the heat for decomposition, resulting in another rapid temperature drop. Moreover, as the corn straw blending ratio increases, the $9.18 < Z < 18.35$ meter region of the furnace has a significant decrease in temperature overall. The average gas temperature at the outlet undergoes a slight decrease, which is consistent with the observations in fig. 5. This phenome-

non may be attributed to the lower calorific value, higher moisture content, and reduced fixed carbon content of corn straw compared to coal powder. Specifically, the precalciner ‘s outlet gas’s average temperature decreases from 1154 K in the absence of biomass to 1152 K, 1150 K, 1147 K, and 1145 K when blended with 10%, 20%, 30%, and 40% corn straw, respectively.

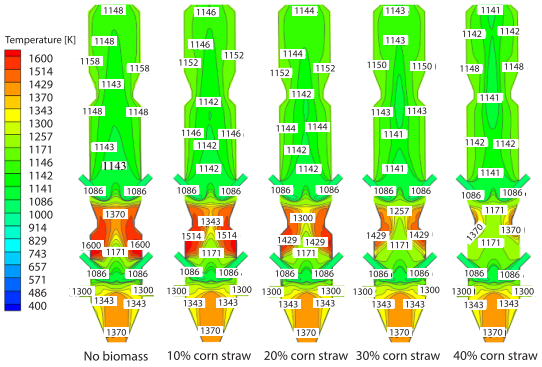

Figure 5. Temperature contour map of the $x = 0$ section in the precalciner under various corn straw blending ratios

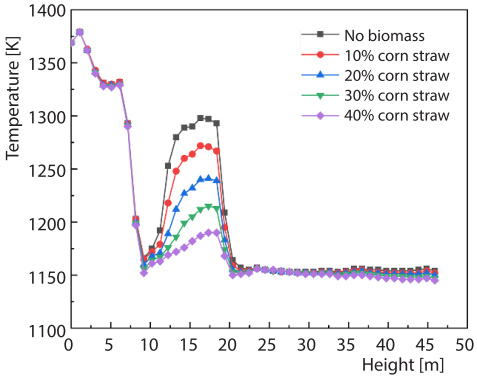

Figure 6. Average gas temperature at various corn straw blending ratios along the precalciner ‘s height

Influence on raw material decomposition

Figures 7 and 8 illustrate the average mass fractions of $CaCO_3$ and CaO at different heights in the precalciner when blending different proportions of corn straw, respectively. The $CaCO_3$ mass fraction in the precalciner exhibits a consistent trend with height. This trend is characterized by an overall pattern of initial increase followed by a decrease, then another increase and subsequent decrease. The mass fraction of $CaCO_3$ increases twice, primarily due to the arrangement of two raw material pipes in the lower and middle sections of the precalciner. In contrast, the mass percentage of CaO on average demonstrates a gradual increasing trend with height. This illustrates the continuous breakdown of raw materials once they enter the furnace, with the average mass fraction of CaO reaching its maximum value at the precalciner‘s outlet. In the range of 19.37 m < z < 20.39 m, there is a brief decrease in the mass fraction of CaO. This

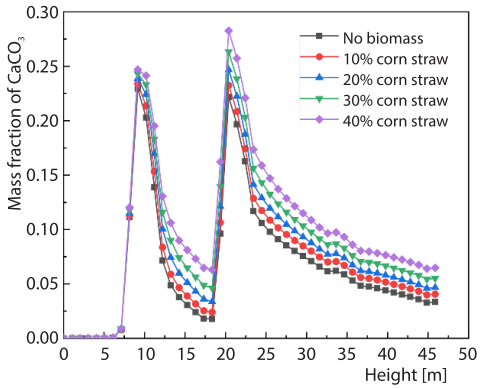

Figure 7. Average $CaCO_3$ mass fraction along the precalciner height for various corn straw blending ratios

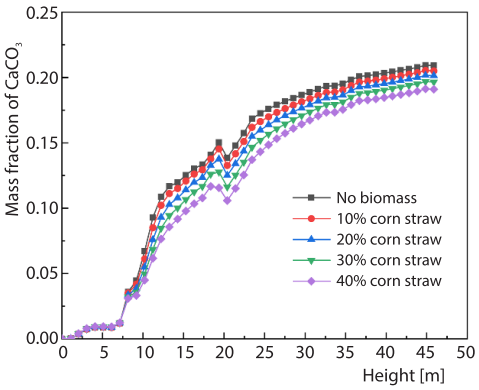

Figure 8. Average CaO mass fraction along the precalciner height at various corn straw blending ratios

is due to some $CaCO_3$ entering the furnace from the upper raw material pipe, which causes a dilution effect on the CaO mass fraction.

Additionally, as the proportion of corn straw replacing coal powder increases. The overall $CaCO_3$ mass fraction in the precalciner gradually increases at heights between 9.18 m and 18.35 m and above 20.39 m. Meanwhile, the overall CaO mass fraction exhibits a gradual decrease. The increase in the proportion of corn straw replacing coal powder results in a gradual decrease in the overall temperature inside the furnace. Consequently, this leads to a reduction in the decomposition rate of raw materials. Calculations reveal that the rates of $CaCO_3$ breakdown at the precalciner 's outlet were found to be 92.31%, 90.21%, 88.40%, 86.31%, and 83.92% when corn straw was blended at ratios of 0%, 10%, 20%, 30%, and 40%, respectively. Considering the requirement in actual production maintain the rate of raw material breakdown at the outlet of the precalciner between 85% and 95%. It is recommended to utilize corn straw as a replacement for pulverized coal at a ratio of 30%, which is more appropriate.

Influence on composition fields

Figures 9 and 10 show the distribution of O_2 and CO_2 on the $x = 0$ section of the precalciner with varying corn straw proportions. These figures indicate that in the absence of biomass, the high concentration area of O_2 is concentrated near the tertiary air inlet, and as the height of the furnace rises, the O_2 concentration gradually decreases. In the main burning area, O_2 is rapidly and significantly consumed, while coal combustion and raw material decomposition release a substantial amount of CO_2, resulting in a higher CO_2 concentration in this area. In the middle and upper columns, O_2 continues to be gradually consumed by unburned coal, resulting in a further drop in O_2 concentration and a rise in CO_2 concentration, with more CO_2 accumulating in the upper column. Moreover, the figures clearly show that as the proportion of corn straw replacing coal powder increases, the high concentration area of CO_2 in the main burning area is significantly reduced. At the same time, the high concentration area of O_2 is significantly increased. This phenomenon may be attributed to the higher oxygen and lower carbon content of corn straw in comparison coal powder, requiring less O_2 and releasing less CO_2 for combustion. Furthermore, the reduction in the raw material decomposition rate also results in a decrease in the CO_2 released.

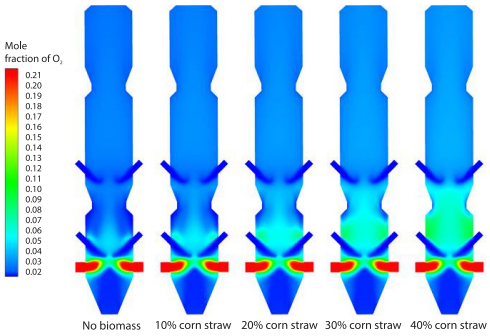

Figure 9. The O_2 distribution map on the $x = 0$ section in the precalciner under various corn straw blending ratios

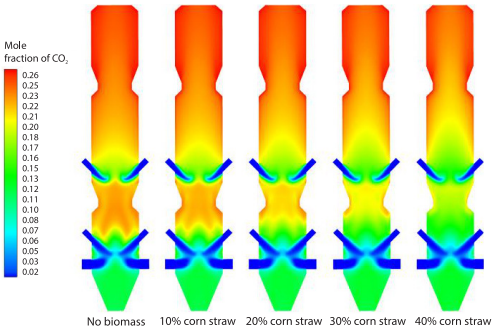

Figure 10. The CO_2 distribution map on the $x = 0$ section in the precalciner under various corn straw blending ratios

Figures 11 and 12 illustrate the average mole fractions of O_2 and CO_2 at different heights in the precalciner when blending different proportions of corn straw, respectively. These figures demonstrate that the trend of changes in the mole percentage of O_2 and CO_2 is opposite,

with the mole fraction of O_2 showing an initial increase followed by a decrease, while the CO_2 mole fraction initially decreases and then increases. This is because the introduction of tertiary air initially increases the O_2 concentration and decreases the CO_2 concentration. Subsequently, as combustion and raw material decomposition proceed, O_2 is gradually consumed and CO_2 is progressively produced. The mole percentage of O_2 reaches its lowest point at the outlet, while the mole percentage of CO_2 reaches its highest point. Additionally, as the proportion of corn straw replacing coal powder increases, the mole percentage of O_2 in the precalciner increases overall after $z > 7.14$ m, while the mole percentage of CO_2 reduces overall. This corresponds to figs. 9 and 10. Specifically, the mole percentage of CO_2 at the exit decreased from 0.2544 without biomass to 0.2319 when mixed with 40% corn straw, indicating that replacing some coal powder with corn straw can reduce carbon emissions. Similarly, Ghenai and Janajreh [18] observed in their numerical simulation study of coal and biomass co-combustion that co-firing can also reduce CO_2 emissions at the furnace outlet.

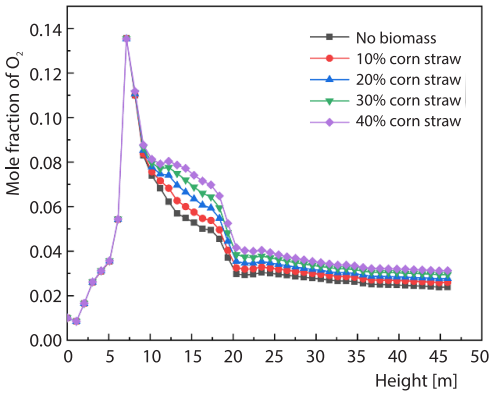

Figure 11. Average O_2 mole fraction along the precalciner height at various corn straw blending ratios

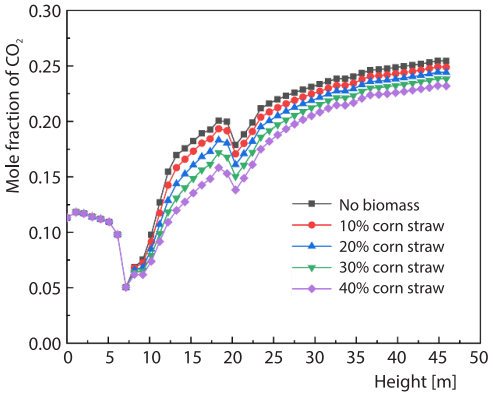

Figure 12. Average CO_2 mole fraction along the precalciner height at various corn straw blending ratios

Influence on NO_x compounds

The two primary sources of NO_x in the precalciner are the fuel NO_x, which is formed by burning fuel, and the thermal NO_x, which is present in the high temperature flue gas at the kiln tail. In this study, the nitrogen contained in the fixed carbon and volatile matter in the fuel is considered to simulate the formation of fuel type NO_x. Figure 13 illustrates the NO distribution on the $x = 0$ section in the precalciner for various corn straw blending proportions. As indicated by fig. 13, the high concentration area of NO in the precalciner is primarily concentrated in the primary combustion area between the inlet of the kiln tail gas and the upper and lower raw material pipes. Furthermore, as the corn straw blending ratio increases, the high concentration area of NO in the main burning area significantly narrows, with the highest concentration of NO decreasing from 793 ppm without biomass to 477 ppm when blending 40% corn straw. This is mainly because corn straw have a lower nitrogen content. The center and upper columns' NO concentration progressively drop as the corn straw blending ratio rises.

Figure 14 presents the average concentration of NO at different heights in the precalciner when blending with different proportions of corn straw. As indicated by fig. 14, at the entrance of the kiln tail gas, the average concentration of NO reaches its maximum value of 583 ppm. Subsequently, as the height increases, the NO concentration rapidly decreases, reach-

ing its lowest point at z = 9.18 m. This rapid decrease can be attributed to the significant dilution effect on NO concentration caused by the large amount of air entering from the third wind. After z > 9.18 m, the NO concentration rises rapidly again, peaking at z = 18.35 m. This increase is due to the rapid oxidation reaction between the fixed carbon and nitrogen in the volatile matter of the fuel and oxygen in the main combustion zone, leading to a continuous increase in NO concentration. At 18.35 m < z < 20.39 m, a brief decrease in NO concentration is observed, which can be attributed to the dilution effect of CO_2 generated by the decomposition of $CaCO_3$ entering the upper raw material pipe on the NO concentration. After z > 20.39 m, as the remaining nitrogen in the fixed carbon and volatile matter continues to oxidize, the NO concentration continues to increase with height and tends to stabilize. It is noteworthy that as the proportion of corn straw replacing coal powder increases, the overall NO concentration in the precalciner gradually drops. At the outlet, the average NO concentration dropped from 507 ppm without biomass to 495 ppm, 490 ppm, 476 ppm, and 464 ppm when mixed with 10%, 20%, 30%, and 40% corn straw, respectively. This finding suggests that replacing a portion of the coal powder with corn straw can effectively reduce the emission of nitrogen oxides. Both Ghenai and Janajreh [18] and Wang *et al.* [19] in their numerical simulations of biomass and pulverized coal co-combustion, found that co-firing reduced NO_x emissions.

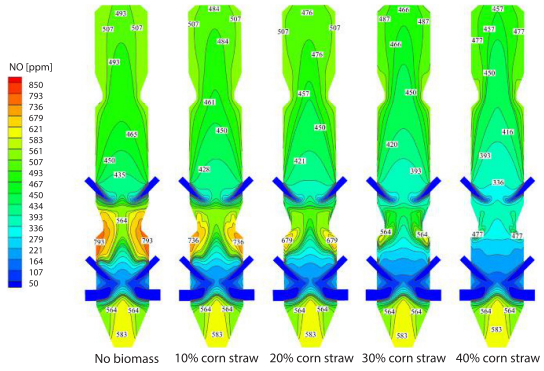

Figure 13. The NO contour map on the x = 0 section in the precalciner under various corn straw blending ratios

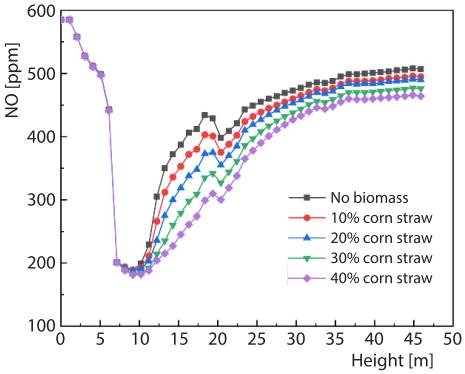

Figure 14. The NO concentration (ppm) at various corn straw blending ratios along the precalciner's height

Conclusions

This study investigated the co-combustion of biomass and pulverized coal in a precalciner. Based on model validation and comparisons with existing research, the following conclusions and future directions are drawn.

- The blending ratio of corn straw significantly impacts the temperature distribution inside the precalciner. As the percentage of corn straw grows, the high temperature zone shrinks, the peak temperature decreases, and the overall temperature inside the furnace gradually reduces. Without corn straw, the maximum temperature reached 1600 K. However, when blended with 40% corn straw, the maximum temperature dropped to 1370 K, and the average outlet gas temperature decreased from 1154 K to 1145 K.
- The decomposition rate of raw materials at the outlet of the precalciner is inversely proportional to the blending ratio of corn straw. Without corn straw, the decomposition rate was 92.31%. As the blending ratio increased to 10%, 20%, 30%, and 40%, the decomposition

rates decreased to 90.21%, 88.40%, 86.31%, and 83.92%, respectively. The average mass fraction of CO_2 at the outlet also reduced from 0.2544 without corn straw to 0.2319 when mixed with 40% corn straw. Similarly, the average concentration of NO at the outlet decreased from 507 ppm without corn straw to 464 ppm when mixed with 40% corn straw. Considering both production requirements and pollution gas emission reduction, a blending ratio of 30% corn straw is deemed more appropriate.

- Since particle size directly affects combustion, further consideration can be given to the impact of biomass particle size on co-combustion. Additionally, the injection position of the biomass can also directly influence combustion within the furnace. It would be valuable to investigate the effects of adding biomass at different positions on the performance of the precalciner.

References

[1] Ali, M. B., *et al*., A Review on Emission Analysis in Cement Industries, *Renewable and Sustainable Energy Reviews*, *15* (2011), 5, pp. 2252-2261
[2] Andrew, R. M., Global CO_2 Emissions from Cement Production, *Earth System Science Data*, *10* (2018), 1, pp. 195-217
[3] Zheng, C., *et al*., Characteristics of CO_2 and Atmospheric Pollutant Emissions from China's Cement Industry: A Life-Cycle Perspective, *Journal of Cleaner Production*, *282* (2021), 124533
[4] Wu, H., *et al*., Experimental Investigation of Cutting Nitrogen Oxides Emission from Cement Kilns Using Coal Preheating Method, *Journal of Thermal Science*, *30* (2021), 4, pp. 1097-1107
[5] Kapitonov, I. A., *et al*., Development of Experience in the Application of Technologies in the Field of Alternative Energy: World Experience, Russian Practice, *Renewable Energy*, *165* (2021), Part 1, pp. 773-782
[6] Pedersen, M. N., *et al*., Imaging of Flames in Cement Kilns to Study the Influence of Different Fuel Types, *Energy & Fuels*, *31* (2017), 10, pp. 11424-11438
[7] Kanevce, G., *et al*., Optimal Usage of Biomass for Energy Purposes Toward Sustainable Development – A Case of Macedonia, *Thermal Science*, *20* (2016), Suppl. 1, pp. S77-S91
[8] Sotoude, M. Y., *et al.*, Analysis of Steady and Oscillating Flames Fueled by Biomass Particles and Syngases Considering Two-Step Pyrolysis and Heterogeneous and Homogeneous Reactions, *International Journal of Hydrogen Energy*, *47* (2022), 51, pp. 21841-21862
[9] Li, P., *et al*., Biological Pretreatment of Corn Straw for Enhancing Degradation Efficiency and Biogas Production, *Bioengineered*, *11* (2020), 1, pp. 251-260
[10] Ren, J., *et al*., Methanation of Syngas from Biomass Gasification: An Overview, *International Journal of Hydrogen Energy*, *45* (2020), 7, pp. 4223-4243
[11] Galina, N. R., *et al.*, Comparative Study on Combustion and Oxy-Fuel Combustion Environments Using Mixtures of Coal with Sugarcane Bagasse and Biomass Sorghum Bagasse by the Thermogravimetric Analysis, *Journal of the Energy Institute*, *92* (2019), 3, pp. 741-754
[12] Yi, B., *et al*., Investigation on the Co-Combustion Characteristics of Multiple Biomass and Coal under O_2/CO_2 Condition and the Interaction between Different Biomass, *Journal of Environmental Management*, *325* (2023), 116498
[13] Sun, J., *et al.*, Computational Fluid Dynamics Modelling of Biomass Co-Firing in a 300 MW Pulverized Coal Furnace, *Thermal Science*, *26* (2022), 5B, pp. 4179-4191
[14] Jeong, H. M., *et al*., Pyrolysis Kinetics of Coking Coal Mixed with Biomass under Non-Isothermal and Isothermal Conditions, *Bioresource Technology*, *155* (2014), Mar., pp. 442-445
[15] Li, L., *et al*., Release of Sulfur and Nitrogen during Co-Pyrolysis of Coal and Biomass under Inert Atmosphere, *ACS Omega*, *5* (2020), 46, pp. 30001-30010
[16] Yuan, Y., *et al*., Co-Combustion Behavior, Kinetic and Ash Melting Characteristics Analysis of Clean Coal and Biomass Pellet, *Fuel*, *324* (2022), Part C, 124727
[17] Mikulčić, H., *et al*., Numerical Study of Co-Firing Pulverized Coal and Biomass Inside A Cement Calciner, *Waste Management & Research*, *32* (2014), 7, pp. 661-669
[18] Ghenai, C., Janajreh, I., The CFD Analysis of the Effects of Co-Firing Biomass with Coal, *Energy Conversion and Management*, *51* (2010), 8, pp. 1694-1701
[19] Wang, X., *et al*., Numerical Study of Biomass co-Firing under Oxy-MILD mode, *Renewable Energy*, *146* (2020), Feb., pp. 2566-2576

[20] Jia, X., *et al.*, Investigation of the Pollutant Emission Characteristics of Blends of Biomass and Coal Gangue in a Fluidized Bed, *Thermal Science*, *26* (2022), 5B, pp. 4333-4343
[21] Black, S., *et al*., Effects of Firing Coal and Biomass under Oxy-Fuel Conditions in a Power Plant Boiler Using CFD Modelling, *Fuel*, *113* (2013), Nov., pp. 780-786
[22] Kim, J., *et al*., Improvement in Reactivity and Pollutant Emission by Cofiring of Coal and Pretreated Biomass, *Energy & Fuels*, *33* (2019), 5, pp. 4331-4339
[23] Oladejo, J., *et al*., Biomass Constituents' Interactions with Coal during co-Firing, *Energy Procedia*, *158* (2019), Feb., pp. 1640-1645
[24] Chansa, O., *et al*., Study of the Kinetic Behaviour of Biomass and Coal during Oxyfuel co-Combustion, *Chinese Journal of Chemical Engineering*, *28* (2020), 7, pp. 1796-1804
[25] Mei, S., *et al*., Numerical Simulation of the Complex Thermal Processes in a Vortexing Precalciner, *Applied Thermal Engineering*, *125* (2017), Oct., pp. 652-661
[26] Cai, R., *et al*., Recent Advances in High-Fidelity Simulations of Pulverized Coal Combustion, *Advanced Powder Technology*, *31* (2020), 7, pp. 3062-3079
[27] Williams, J. J. R., Free-Surface Simulations Using an Interface-Tracking Finite-Volume Method with 3-D Mesh Movement, *Engineering Applications of Computational Fluid Mechanics*, *1* (2007), 1, pp. 49-56
[28] Corcoles, J. I., *et al*., Influence of Corrugation Shape on Heat Transfer Performance in Corrugated Tubes Using Numerical Simulations, *International Journal of Thermal Sciences*, *137* (2019), Mar., pp. 262-275
[29] Ophoff, C., *et al*., A Numerical Study on Particle Tracking and Heat Transfer Enhancement in a Solar Cavity Receiver, *Applied Thermal Engineering*, *180* (2020), 115785
[30] Shuang, Y., *et al.*, Heat Transfer Inside Particles and Devolatilization for Coal Pyrolysis to Acetylene at Ultrahigh Temperatures, *Energy & Fuels*, *24* (2010), 5, pp. 2991-2998
[31] Choi, C. R., Kim, C. N., Numerical Investigation on the Flow, Combustion and NO_x Emission Characteristics in a 500 MWe Tangentially Fired Pulverized-Coal Boiler, *Fuel*, *88* (2009), 9, pp. 1720-1731

Paper submitted: July 22, 2024
Paper revised: September 18, 2024
Paper accepted: November 1, 2024